

Nanoscale

Accepted Manuscript



This is an *Accepted Manuscript*, which has been through the Royal Society of Chemistry peer review process and has been accepted for publication.

Accepted Manuscripts are published online shortly after acceptance, before technical editing, formatting and proof reading. Using this free service, authors can make their results available to the community, in citable form, before we publish the edited article. We will replace this *Accepted Manuscript* with the edited and formatted *Advance Article* as soon as it is available.

You can find more information about *Accepted Manuscripts* in the [Information for Authors](#).

Please note that technical editing may introduce minor changes to the text and/or graphics, which may alter content. The journal's standard [Terms & Conditions](#) and the [Ethical guidelines](#) still apply. In no event shall the Royal Society of Chemistry be held responsible for any errors or omissions in this *Accepted Manuscript* or any consequences arising from the use of any information it contains.



Journal Name

ARTICLE

Bi-phasic titanium dioxide nanoparticles doped with nitrogen and neodymium for enhanced photocatalysis

V. Gomez,^{a†} J. C. Bear,^{a†} P. D. McNaughten,^b J. D. McGettrick,^c Trystan Watson,^c C. Charbonneau,^c Paul O'Brien,^{b,d} Andrew R. Barron,^{a,e} and Charles W. Dunnill^{a*}

Received 00th January 20xx,
Accepted 00th January 20xx

DOI: 10.1039/x0xx00000x

www.rsc.org/

Bi-phasic or multi-phasic composite nanoparticles for use in photocatalysis have been produced by a new synthetic approach. Sol-gel methods are used to deposit multiple layers of active material onto soluble substrates. In this work, a layer of rutile (TiO₂) was deposited onto sodium chloride pellets followed by an annealing step and a layer of anatase. After dissolving the substrate, bi-phasic nanoparticles containing half anatase and half rutile TiO₂; with “Janus-like” characteristics are obtained. Nitrogen and neodymium doping of the materials were observed to enhance the photocatalytic properties both under UV and white light irradiation. The unique advantage of this synthetic method is the ability to systematically dope separate sides of the nanoparticles. Nitrogen doping was found to be most effective on the anatase side of the nanoparticle while neodymium was found to be most effective on the rutile side. Rhodamine B dye was effectively photodegraded by co-doped particles under white light.

1. Introduction

Multi-phasic composite materials have long been of interest for a vast array of applications from solar cells and energy harvesting^{1–5} to medicine and imaging^{6–9} and catalysis.^{10–14} Having two or more materials in intimate contact allows the benefits of both along with synergistic interactions such as the provision of electrons,^{14, 15} alteration of absorption/emissive properties,¹⁶ increasing mechanical strength¹⁷ and impact resistance.¹⁸

Herein we present a facile method for the deposition of multiple layered composite nanoparticles based on sequential deposition using sol-gel chemistry and soluble substrates. Water soluble salts such as sodium chloride and sodium fluoride are easily compressed into pellets on which layers of material can be deposited through standard thin film methods such as sol-gel. Essentially the process involves depositing a layer of material onto a soluble substrate, annealing to fix the

layer before depositing a different layer on to and then removing the substrate. The thin films then fracture to yield composite nanoparticles.

Sol-gel chemistry represents a facile pathway for the formation of thin films via dip, spin and spray-coating.^{19–21} In this study we employ a series of dip-coating steps in a sol of the precursors of our desired material, which consists of Janus like particles containing doped phases of titanium oxide in both its anatase and rutile forms. A single layer of titanium oxide can be applied to a soluble substrate before an annealing step which crystallizes the material into the desired rutile form, before a subsequent layer is deposited using the same method, by dip-coating with another sol, or by varying the annealing temperature as in the synthesis of rutile/anatase TiO₂ junctions where a crystal phase transition occurs at 600 °C.^{22,23}

After sequential depositions and desired annealing stages, the substrate is then dissolved in water causing the films formed on the surface of the substrate to fragment into layered bi-phasic nanoparticles. The biggest advantage of this method is the range of materials available via sol-gel processes and the composite materials that can be envisaged and created. We also demonstrate that the general method is robust enough to support nitrogen and neodymium doped films, increasing the versatility of the method even further, and allowing real control over the individual phases within the biphasic system. Using anatase/rutile junctions as a case study we show the proficiency of this method to generate bi-phasic, junctioned doped and undoped nanoparticles for photocatalytic water purification and other photocatalytic applications.

^a Energy Safety Research Institute (ESRI), College of Engineering, Swansea University, Bay Campus, Fabian Way Swansea, SA1 8EN, UK. Email: c.dunnill@swansea.ac.uk

^b School of Chemistry, University of Manchester, Oxford Road, Manchester, M13 9PL, UK.

^c A SPECIFIC, College of Engineering, Swansea University, Baglan Bay Innovation and Knowledge Centre, Central Avenue, Baglan, Port Talbot, SA12 7AX, UK.

^d School of Materials, University of Manchester, Oxford Road, Manchester, M13 9PL, UK.

^e Department of Chemistry and Department of Materials Science and Nanoengineering, Rice University, Houston, Texas 77005, USA.

† These authors contributed equally to this work.

Electronic Supplementary Information (ESI) available: [details of any supplementary information available should be included here]. See DOI: 10.1039/x0xx00000x

Titanium dioxide has been and continues to be the key material in the development of photocatalysts for a myriad of applications including: water-splitting for hydrogen production,^{24–27} anti-microbial and self-cleaning surfaces,^{28–33} solar cells^{34–36} and water purification.^{35–39} The need to maximize the Earth's resources and the ever-increasing need for energy has been the catalyst for titanium dioxide research, and has in turn led to intensive study and rapid development, primarily due to titanium's earth abundance, high activity and cost-effectiveness.^{42–44}

The synergistic effects between anatase and rutile titanium dioxide has been exploited by several groups for enhanced photocatalysis compared to anatase or rutile phases alone,^{45–47} but it wasn't until recently that the exact mechanism of activity and band alignment was determined⁴⁸ and confirmed using photocatalytic tests.⁴⁹ Scanlon *et al.* used density functional theory, X-Ray photoelectron spectroscopy and existing electron paramagnetic resonance data which supported the hypothesis that electrons move from rutile to anatase, to demonstrate that a de facto type (II) staggered band alignment of ~0.4 eV exists in anatase-rutile junctions, thus leading to superior separation of charge carriers compared to the individual phases.⁴⁸ The separation of charge enhances the lifetime of the excited state and improves the photocatalytic properties. In this way the anatase stabilizes the rutile and the rutile stabilizes the anatase and thus a synergistic arrangement is apparent. Given that the electrons concentrate on the anatase whilst the holes concentrate on the rutile, both phases play intrinsically different roles in the overall redox reaction that is the photo catalysis. The anatase with its concentration of electrons acts as a reduction catalyst whilst the rutile with its concentration of holes acts as an oxidation catalyst.

Doping titania systems to increase their performance in photocatalysts has been exhaustively investigated, with numerous metal and semi-metal dopants shown to be effective. In particular, nitrogen has received a great deal of attention due to the effect interstitial nitrogen has on the anatase titania lattice and overall bandgap of the material, which unlocks visible light absorption through the formation of intra-band states.^{50,51} As well as the formation of intra-band states, dopants may also introduce oxygen vacancies in the titania lattice which aids the absorption of visible light or act as trap states, prolonging the lifetime of the exciton.^{19,40,52–54}

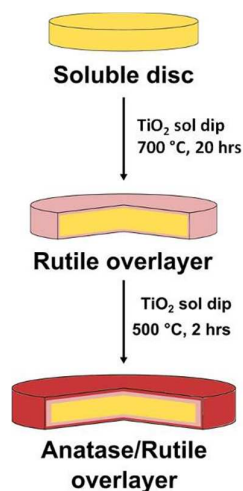
The TiO₂ lattice has a relatively high tolerance for doping, and as such, transition metal dopants are routinely used to replace the Ti⁴⁺ cation, such as W,⁵⁵ V,⁵⁶ Zr,⁵⁷ Fe^{58,59} and Cu.⁶⁰ f-block elements such as La and Ce are well known for their enhancement of the photocatalytic properties of TiO₂, due to the effect of the presence of vacant f-orbitals which facilitate the generation of intermediate energy states. La-doped anatase TiO₂ inhibits the temperature induced phase transition to rutile.^{61,62} Neodymium (Nd³⁺) as a dopant for titania systems has been shown to be similar to that of other rare earth dopants, with successful application in photocatalysis and dye-

sensitised solar cells.^{40,52,63,64} Nd-doped TiO₂ composites have been shown by several groups to enhance the photocatalytic degradation of waste water contaminants under visible light irradiation, such as 4-nitrophenol,⁶⁴ 2-chlorophenol,⁶⁵ [partially hydrolysed] poly(acrylamide)⁶⁶ and n-butylamine.⁶⁷ Using a sequential-layer deposition technique onto water soluble substrates, we present the synthesis of neodymium doped bi-phasic titania nanoparticles demonstrating improved photocatalytic activity under UV (365 nm) and visible irradiation for the photodegradation of Rhodamine B in water. The nanoparticles are synthesized by the deposition of a rutile layer onto a soluble substrate. The substrate could be any one of a number of high-melting point inorganic materials, but for this study we chose NaCl due to its high melting point (mp 801 °C) and high solubility in water (solubility 360.9 g/L of water at 303 K). Deposition of a rutile titania layer was followed by an anatase layer. Therefore, when the substrate is dissolved, the bi-phasic titania nanoparticles are easily isolated due to the insolubility of TiO₂ in aqueous systems. We then demonstrate the enhanced synergistic photocatalytic activity afforded by rutile-anatase junctions with Nd and N double doping under white light compared to undoped and single doped anatase and rutile systems. It is also demonstrated that the nanoparticles can be easily isolated from aqueous systems by either simple filtration or centrifugation. This is therefore a controlled method for the evaluation of doped rutile-anatase junctioned nanoparticles / microparticles for the treatment of organic contaminants in waste water.

2. Experimental

Materials and methods.

Janus like, biphasic particles containing 2 phases of TiO₂, (anatase and rutile), intimately connected were prepared by sequential layer deposition onto soluble substrates which were subsequently removed / dissolved away.⁶⁸ The multistep synthesis involved pressing pellets of sodium chloride to create the substrates, preparing titanium dioxide Sol gels, in pure form and with both neodymium and nitrogen doping elements and sequential deposition by dip coating the sols onto the substrates, (Scheme 1)



Scheme 1 Scheme detailing the synthesis of the rutile/anatase titania composite upon a soluble substrate. This process can be applied to any sol-gel synthesis using a vast array of substrate materials.

Neodymium nitrate hexahydrate (99.9% trace metal basis), Rhodamine B, sodium chloride (ReagentPlus®, ≤95%), N,N,N',N'-tetramethylethylenediamine (ReagentPlus®, 99 %), titanium(IV) butoxide (reagent grade, 97%) and titanium(IV) oxide, anatase powder, -325 mesh, ≥99% trace metals basis were purchased from Sigma Aldrich Ltd. Acetylacetone (AnalaR), acetonitrile (AnalaR), 1-butanol (98.5%), 2-Propanol (tech. grade) and sodium fluoride (99%) were purchased from VWR Ltd.

All other solvents used were of the highest possible grade and purchased from Sigma-Aldrich Ltd. UHQ Deionised water with a resistivity of not less than 18.2 MΩ cm⁻¹ (Millipore) was used for aqueous solutions and substrate dissolution.

Preparation of soluble substrates. Substrates were prepared by subjecting finely ground sodium chloride (~1 g) or sodium fluoride (~1 g) to ~7 T of pressure in a 12 mm dye press (Retch PP 55 with a pressure of ca. 8 tons) for 10 minutes, creating homogeneous pellets.

Titania sol synthesis. Titania sols were prepared using the protocol developed by Powell *et al.*⁶⁹ with modifications. Briefly, titanium(IV) butoxide (50 mmol, 17.0 mL) was added to a mixture of acetylacetone (25 mmol, 2.57 mL) and 1-butanol (50 mmol, 4.58 mL) under vigorous stirring, giving a transparent yellow sol. After 1 hour, a mixture of 2-propanol (150 mmol, 11.5 mL) and deionised water (3.64 mL) was added before further stirring for 1 hour. Acetonitrile (40 mmol, 2.09 mL) was then added and the whole system sealed and allowed to age overnight (ca. 10 hours) before dip-coating. Sols were stable up to 6 months if stored in an air-tight container. (Samples **R/A**, **N-R/A** and **R/N-A**)

N-doped titania sol synthesis. To affect nitrogen doping, the sol was prepared using the titania sol synthesis, but with the addition of N,N,N',N'-tetramethylethylenediamine (12.9 mmol, 1.93 mL) with the acetonitrile to create the N-doped sol, according to Powell *et al.*⁶⁸ (Samples **N-R/A**, **R/N-A** and **N-R/N-A**)

Nd-doped titania sol synthesis. To affect neodymium doping (e.g. 3 % Nd-doping), the sol was prepared using the titania sol synthesis, but with the inclusion of neodymium nitrate hexahydrate (1.5 mmol, 0.658 g) in the water/2-propanol mixture to create the Nd-doped sol. The quantity of titanium(IV) butoxide was also adjusted to (48.5 mmol, 16.5 mL) It is noteworthy that the Nd-doped titania sol was a transparent yellow overall with a blue tint. (Samples **Nd-R/A**, **R/Nd-A** and **Nd-R/Nd-A**)

N-doped-Nd-doped titania sol synthesis. To affect nitrogen and neodymium doping, the sol was prepared using the titania sol synthesis, but with the inclusion of neodymium nitrate hexahydrate (1.5 mmol, 0.658 g) in the water/2-propanol mixture and N,N,N',N'-tetramethylethylenediamine (12.9 mmol, 1.93 mL) with the acetonitrile to create the N-doped-Nd-doped TiO₂ sol. The quantity of titanium(IV) butoxide was also adjusted to (48.5 mmol, 16.5 mL). (Sample **N-Nd-R/N-Nd-A**)

Synthesis of bi-phasic layers: Sodium chloride pellets were completely immersed in one of the aforementioned titania sols for two seconds. Coated pellets were dried in an oven at 80 °C. This was repeated twice before annealing in a furnace for 20 hours at 750 °C to form a crystalline rutile titania layer and cooled to room temperature naturally.

On cooling, the coated pellets were immersed in the desired titania sol (for the second [anatase] layer) and dried at 80 °C; again repeated twice. The pellets were annealed in a furnace for 2 hours at 500 °C to form the crystalline anatase titania layer.

The coated pellets were added to distilled water and centrifuged at 1000 × *g* to retain the bi-phasic titania nanoparticles as the sodium chloride substrates dissolved. The resultant slurry was washed in fresh deionized water and centrifuged six times to ensure complete removal of the soluble substrate.

Photocatalytic dye degradation tests. Rhodamine B was used as a model organic pollutant as it exhibits characteristics of many common pollutants such as aromaticity. Rhodamine B also has strong absorption profile at 550 nm, ideally suited to monitoring by UV-vis spectroscopy.

Photocatalytic measurements were taken at 2 different wavelengths: 365 nm (UV) and 6500K (white light, *vide infra*). A stock solution of Rhodamine B (0.005 mg/mL) in distilled water (100 ml total) was prepared and divided into 6 mL portions in glass vials. Samples of bi-phasic nanoparticles (by weight, 6 mg) were added to each solution before irradiation, and the suspensions stirred throughout. Dispersions were stirred in darkness for 2 h before commencing, so as to

prevent the measurement of dye adherence to the particles as a false-positive result.⁷⁰ In addition a standard dye sample was maintained under the same conditions as those used in the experiments, but in the absence of photocatalysis so as to be sure of the integrity of the dye under operating conditions. Rhodamine B degradation was measured by UV-VIS spectroscopy against this control solution of Rhodamine B at regular time intervals.

Characterization.

Transmission electron microscopy (TEM) images were recorded using a FEI Tecnai G2 20 with a LaB₆ source at an acceleration voltage of 200 kV. EDS spectra were taken with an Oxford XMax 80 TLE detector running AZTEC software. Samples were characterized by scanning electron microscopy using an Ultra-High Resolution FE-SEM S-4800 coupled with an energy dispersive X-ray analyzer (Inca X-ray analysis system, Oxford Instruments, Abingdon, UK) was used for the EDS. UV-vis absorption spectra were recorded using a Thermo Electron Corporation UNICAM UV300 UV/Vis spectrometer. X-Ray diffraction (XRD) patterns were recorded on a Brüker d8 DISCOVER diffractometer with a Cu K α X-Ray source ($\lambda = 0.15418$ nm and analyzed using Match 2 software. X-Ray photoelectron spectra (XPS) were recorded on a Kratos Axis Supra instrument (Kratos Analytical, Manchester, UK) using a monochromated Al K α source. All spectra were recorded using a charge neutralizer to limit differential charging and subsequently calibrated to the main C_{1s} carbon peak at a binding energy of 284.8 eV. Survey scans were recorded at a pass energy of 160 eV and high resolution data at a pass energy of 20 eV. Data was fitted using CASA XPS with Shirley backgrounds. For all elements except Nd, the most intense photoelectron peak was used for high-resolution spectroscopy. The relatively weak Nd (3d) peak at a binding energy of ~980 eV is heavily overlapped by the O_{1s} structure, so the Nd(4d) region at 120 eV was chosen in preference. This can be fitted with a single broad peak (FWHM 7.3 eV) or with two smaller peaks (FWHM 5.0 eV) assumed to correspond to the 4d_{3/2} and 4d_{5/2} signals. Diffuse reflectance UV-Vis spectroscopy measurements were performed with a Perkin Elmer Lambda 750S (60 mm integrating sphere). The samples were vertically positioned against the reflectance opening of the integrating sphere so that the centre of the TiO₂ film was aligned with the beam path. The spectra were recorded between 250 and 800 nm with a 2 nm step. Reflectance data was converted into a Kubelka-Munk function and multiplied by the energy at each step using MatLab software for the Tauc plots.

Dye degradation. Photocatalytic dye degradation studies were undertaken using a PLUVEX 1410 UV exposure unit with a working area of 229 × 159 mm with a UV output of 2 × 8 W (2.5 mW/cm²) at a distance of 10 cm from the surface of the sample solutions. For the white light photocatalysis measurements, a lightbox was constructed. The box comprised

an MDF container measuring ~650 mm on three sides of a cube and an internal volume of ~280 liters with internal surfaces coated in 1 mm thick acrylic mirror and housed 5 fluorescent tube lighting assemblies. Each fluorescent tube lighting assembly contained two fluorescent tubes of 600 mm and 18 W white light with a rating of 6500 K. The lightbox totaled 180 W and was temperature controlled to ambient by a fan attached to the side. Samples were placed in glass containers on top of mini steering plates so that these solutions could be agitated whilst under the light source.

3. Results

The dip-coating of the water soluble substrates into titania sols with annealing steps to crystallize separate titania phases is summarized in Scheme 1. The first step details the dipping, of a chosen substrate into a titania sol before drying at 80 °C and annealing at 700 °C to form rutile titania. The process is then repeated, but the annealing temperature lowered to 500 °C in order to form the outer, anatase titania layer.

This method is a facile route for the formation of many different materials, not just constrained to titania. There are advantages when considering hydrogen generation from water, where intimate contact between reduction and oxidation catalysts is essential.

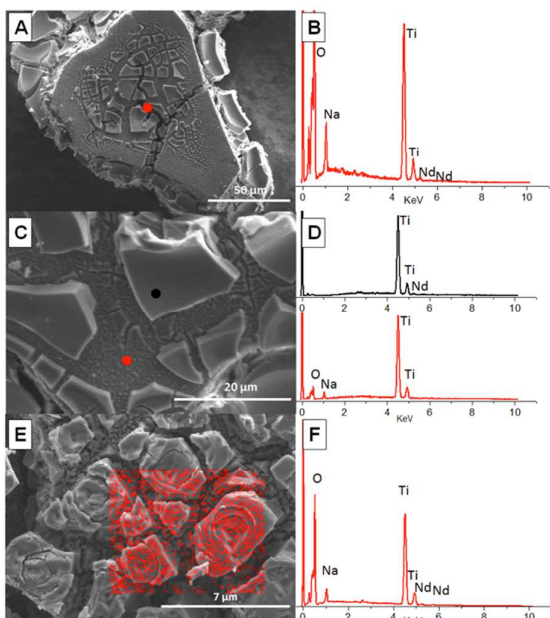
Different dopants - such as nitrogen and neodymium - were added during the sol synthesis. Nitrogen doping was affected through the addition of N,N,N',N'-tetramethylethane-1,2-diamine (TMEDA) after addition of acetonitrile. The good miscibility of TMEDA with 1-butanol facilitated its addition at that stage. Neodymium(III) nitrate however had to be added in a water/isopropanol mix due its solubility in 1-butanol.

With the four methods of doping, all possible combinations of bi-phasic rutile-anatase systems were synthesized and evaluated using UV and white light photocatalytic dye degradation. For a full list of samples see Table S1.

SEM micrographs of the composite material before dissolution show uniform coverage of the pellet by the anatase/rutile composite layers. The harsh reaction and crystallization conditions contributed to the large surface fissures seen across the composite. This morphology is advantageous for substrate dissolution, as it aids water ingress to the surface. EDS analysis by SEM and TEM indicated the presence of titanium and oxygen in the sample. Neodymium doped samples returned doping levels proportionate to the amount of doping solution used (in all samples this was 3% Nd). Figure 1d shows the presence of Nd in the EDS spectrum is only obtained from the upper layer and not the underlying undoped rutile layer, in agreement with the expected structure for sample **R/Nd-A**. Figure 1e shows a SEM micrograph and an EDS mapping area with its related spectrum for sample **Nd-R/Nd-A**, confirming the presence of Nd in both layers. It is also noteworthy that traces of the

soluble substrate (in most cases NaCl) are present in EDS spectra, indicating incomplete removal of the template substrate.

Fig. 1 SEM micrographs and associated EDS analysis of sample **R/Nd-A** (a, b, c and d) and sample **Nd-R/Nd-A** (e and f).



The isolated bi-phasic materials were found to be sub-micron in size, after post-annealing dissolution of the soluble substrates with distilled water. Large, polydisperse aggregates of nanoparticles were seen in TEM images (Figure 2). Average sizes of all samples are tabulated in the supporting information (Table S2). Measured lattice planes from HRTEM indicate that the rutile and anatase phases of titania co-exist, commensurate for the synergistic enhancement of photocatalytic activity seen in anatase/rutile composite materials (Figure 2e) simultaneously showing d -spacings of 0.379 nm and 0.307 nm corresponding to the $\langle 101 \rangle$ of anatase and $\langle 110 \rangle$ of rutile titania respectively).^{48,49} TEM micrographs showed little alteration on doping with nitrogen, neodymium or both, as evidenced in Figure 2.

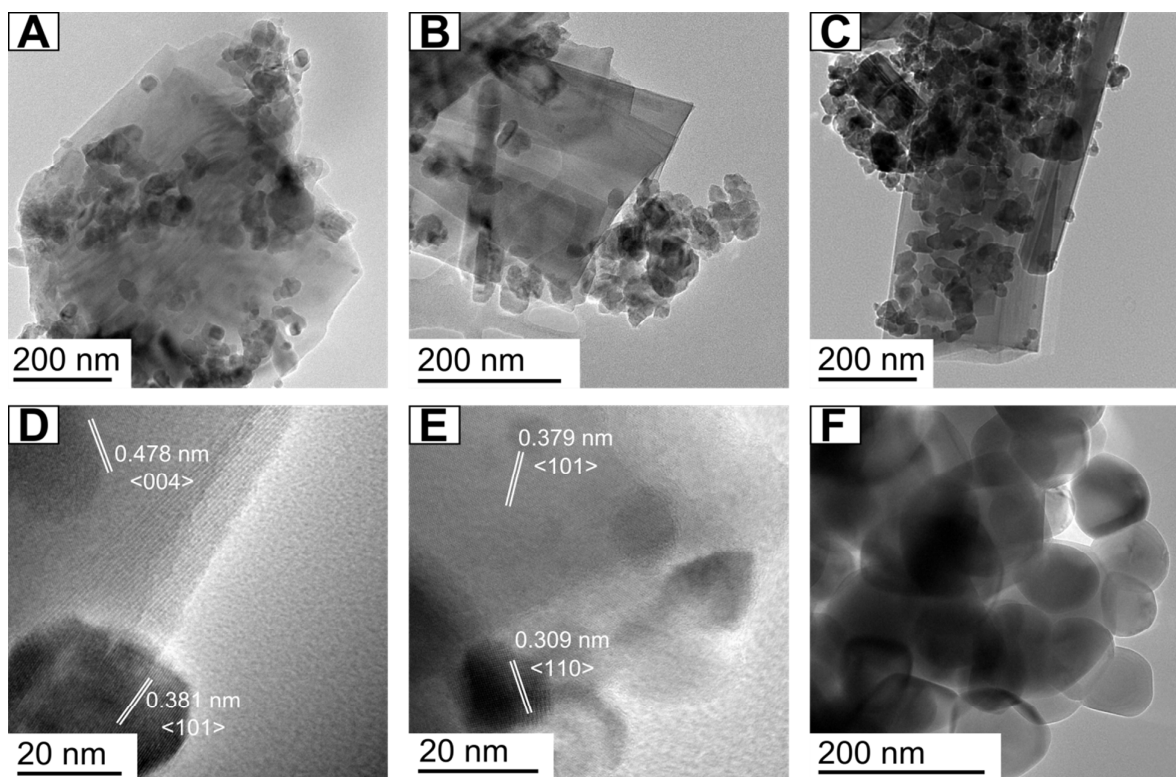


Fig. 2 Transmission electron micrographs of (a) rutile – anatase, (**R/A**), (b) N and Nd doped rutile – N and Nd doped Anatase, (**N-Nd-R/N-Nd-A**), (c) and (d) Nd doped rutile – N and Nd doped anatase, (**Nd-R/Nd-A**), (e) N doped rutile – N doped anatase, (**N-R/N-A**), showing rutile and anatase lattice planes simultaneously and (f) anatase TiO₂ standard.

Particle size measurements obtained from TEM micrographs demonstrated a high degree of polydispersity as evidenced by the large standard deviation values (see Table S2). Polydispersity is a disadvantage of the layering method; however, TEM demonstrates the existence of nanoparticles which are large enough to have distinct phases of different materials, the key objective of this method.

Evidence for the anatase-rutile layered structure was further supported by Raman analysis. A sample of **R/A** was synthesised with 5 layers of rutile and 5 subsequent layers of anatase. The 5 layer **R/A** samples was analysed both in powder form and as a fragment, peeled off the sodium chloride disc. The sample gave a Raman spectrum that was consistent with a mix of both anatase and rutile forms of TiO₂, (figure S1). Peak positions for the R/A sample were assigned as follows (in cm⁻¹): 141.48 (E_g, anatase), 194.95 (E_g, anatase), 395.89 (E_g, anatase), 445.82 (E_g, rutile), 514.1 (B_{1g}, anatase), 613.65 (A_{1g}, rutile), 635.7 (E_g, anatase)."

XPS data for sample **Nd-R/N-Nd-A** are presented in Figure 3 (full quantification is presented in Table S3). The survey scan (Figure 3a) shows the expected O(1s), Ti(2p), N(1s) and Nd(3d & 4d) signals. Additionally, strong Na(1s & KLL) and Cl(2p & 2s) signals indicate some residual NaCl from undissolved substrate. A strong C(1s) signal is also observed. This has been previously observed in Nd-doped TiO₂ from the organic precursors utilized in the sol-gel process,⁷¹ but is also consistent with adventitious carbon contamination.

The position of the Ti(2p_{3/2}) peak (Figure 3c) at a binding energy of 458.3 eV represents 11 at.% of the surface and is consistent with TiO₂, and has previously been observed in both Nd doped TiO₂^{72,73} and N doped TiO₂.⁷⁴ The O (1s) high resolution spectrum is deconvoluted into two peaks (Figure 3d). The main sharp peak at 529.6 eV is consistent with metal oxides in general and this peak represents 22 at. % of the total surface giving a Ti:O (metal oxide) ratio of approximately 2:1. The smaller, broader peak at 530.6 eV is attributed to oxidized organic species from the organic contamination (C-O bonds), but may also include surface hydroxyl species.⁷⁵ For the Nd-doped materials, the Nd (4d) peak is observed at 121.3 eV and has been previously observed to be Nd(III) rather than Nd(0). The observed Nd:Ti ratio is 0.060, which could indicate some enrichment of Nd at the TiO₂ surface.^{76,77} Low levels of nitrogen are observed on most of the samples. In the case of the TiO₂ control sample a tiny (0.04 at. %) N (1s) peak is observed at 406.2 eV, which is attributed to some residual surface NO_x species. For the doped samples larger N(1s) peaks are observed at around 399–400 eV.¹⁹ An extensive discussion of the potential assignment of this peak concludes that it probably represents interstitial N doping in the TiO₂ lattice, although the signal could also be assigned to organic species.²⁹

The isolated bi-phasic materials were found to be sub-micron in size, after post-annealing dissolution of the soluble substrates with distilled water. Large, polydisperse aggregates of nanoparticles were seen in TEM images (Figure 2). Average sizes of all samples are tabulated in the supporting information (Table S2.1). Measured lattice planes from HRTEM indicate that the rutile and anatase phases of titania co-exist, commensurate for the synergistic enhancement of photocatalytic activity seen in anatase/rutile composite materials (Figure 2e) simultaneously showing *d*-spacings of 0.379 nm and 0.307 nm corresponding to the <101> of anatase and <110> of rutile titania respectively).^{48,49} TEM micrographs showed little alteration on doping with nitrogen, neodymium or both, as evidenced in Figure 2.

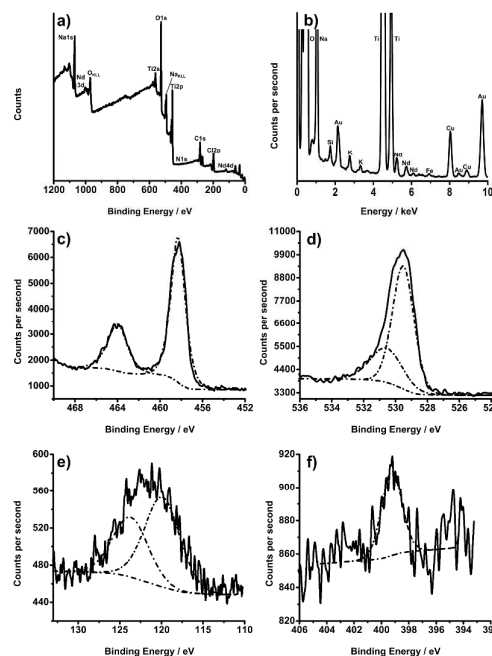


Fig. 3 X-Ray photoelectron spectra of the Nd-R/N-Nd-A sample. (a) Survey scan with Ti, O, Na, Cl, C, N and Nd highlighted, (b) EDS spectrum from TEM of the same sample showing the presence of Ti, O and Nd. Cu, Fe and Au emanated from the microscope goniometer and the TEM grid respectively, and (c-f) high resolution XPS spectra of Ti 2p, O 1s, Nd 3d and N 1s respectively.

Particle size measurements obtained from TEM micrographs demonstrated a high degree of polydispersity as evidenced by the large standard deviation values (see Table S2.1). Polydispersity is a disadvantage of the layering method; however, TEM demonstrates the existence of nanoparticles

which are large enough to have distinct phases of different materials, the key objective of this method.

XPS data for sample **Nd-R/N-Nd-A** are presented in Figure 3 (full quantification is presented in Table S3.1). The survey scan (Figure 3a) shows the expected O(1s), Ti(2p), N(1s) and Nd(3d & 4d) signals. Additionally, strong Na(1s & KLL) and Cl(2p & 2s) signals indicate some residual NaCl from undissolved substrate. A strong C(1s) signal is also observed. This has been previously observed in Nd-doped TiO₂ from the organic precursors utilized in the sol-gel process,⁷¹ but is also consistent with adventitious carbon contamination.

The position of the Ti(2p_{3/2}) peak (Figure 3c) at a binding energy of 458.3 eV represents 11 at.% of the surface and is consistent with TiO₂, and has previously been observed in both Nd doped TiO₂^{72,73} and N doped TiO₂.⁷⁴ The O (1s) high resolution spectrum is deconvoluted into two peaks (Figure 3d). The main sharp peak at 529.6 eV is consistent with metal oxides in general and this peak represents 22 at % of the total surface giving a Ti:O (metal oxide) ratio of approximately 2:1. The smaller, broader peak at 530.6 eV is attributed to oxidized organic species from the organic contamination (C-O bonds), but may also include surface hydroxyl species.⁷⁵ For the Nd-doped materials, the Nd (4d) peak is observed at 121.3 eV and has been previously observed to be Nd(III) rather than Nd(0). The observed Nd:Ti ratio is 0.060, which could indicate some enrichment of Nd at the TiO₂ surface.^{76,77} Low levels of nitrogen are observed on most of the samples. In the case of the TiO₂ control sample a tiny (0.04 at. %) N (1s) peak is observed at 406.2 eV, which is attributed to some residual surface NO_x species. For the doped samples larger N(1s) peaks are observed at around 399–400 eV.¹⁹ An extensive discussion of the potential assignment of this peak concludes that it probably represents interstitial N doping in the TiO₂ lattice, although the signal could also be assigned to organic species.²⁹ XRD diffraction patterns of the undoped, single and double doped TiO₂ samples are shown in Figure 4. The obtained powders showed diffraction peaks at 25.3, 36.9, 37.8, 38.6, 48.1, 53.9, 55.1, 62.7 °2θ anatase (COD 9009086) and at 27.5, 36.1, 41.3, 54.4, 56.7, 62.8, 64.1, 69.1 69.8 2θ rutile (COD 904143). The XRD patterns also show diffraction peaks at 27.3, 31.6, 45.4, 66.2 °2θ NaCl halite phase (COD 9006375). The presence of NaCl in the samples is due to the incomplete removed substrate. The broad diffraction peaks obtained prevented us from observing any shift in the peak maxima that could be ascribed to the incorporation of Nd in the TiO₂ lattice. Due to high temperatures required for rutile and anatase crystallisation, ionic mobility within the “solid” matrix of the sodium chloride occurs, with sodium ions infiltrating the rutile/anatase titania crystal lattices. In the undoped rutile-anatase sample (sample **R/A**) a peak at 24.4 2θ corresponding to the presence of sodium titanate Na₂O₁₃Ti₆ (COD 4000748) can be observed.⁷⁸ Alkaline metal titanates, comprising edge-sharing TiO₆ octahedra with an alkaline cation in between the

crystal layers, have been reported to impart advantageous characteristics for photocatalytic performance.⁷⁹

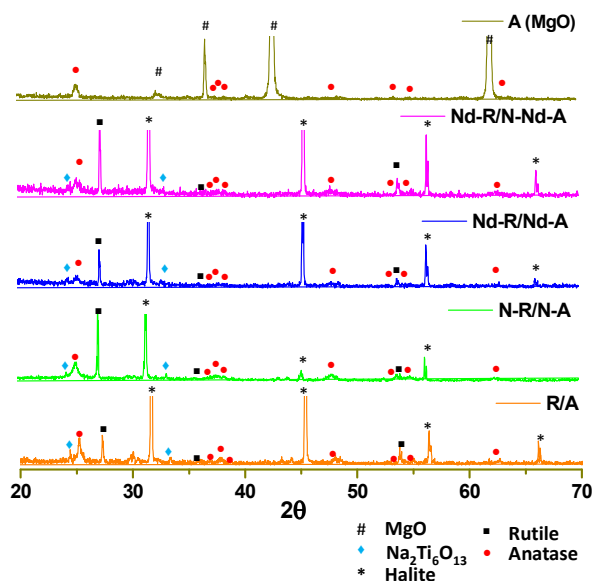


Fig. 4 XRD patterns of undoped, single and double doped titania samples. Main diffraction lines for anatase, rutile, sodium titanate, magnesium oxide and halite sodium chloride phases are indicated.

Different substrates were prepared by depositing a single anatase layer (annealed at 500 °C for 2 hours) onto magnesium oxide (mp 2852 °C). The use of substrates with different solubility and melting points can be advantageous in different applications of the materials. Some desirable combinations of hydrogen catalyst and oxygen catalysts for water splitting reactions and efficient solar energy harvesting could require high temperature process in excess of the 800 °C limit of sodium chloride. Coupled to this is the desire to operate the substrates temperature well below their melting point as this will reduce the ion mobility. The trade-off here however is in the solubility, sodium chloride (360.9 g/L of water at 303 K) far outperforms the near-insoluble magnesium oxide (0.086 g/L of water at 303 K). Acid or base can be used to aid in solubility, depending on the nature of the phases within the composite material. Diffraction patterns of the TiO₂ sample deposited on magnesium oxide are shown in Figure 4. It shows diffraction peaks at 36.81, 42.8, 62.18 °2θ indexing to the magnesium oxide phase (COD 4111968).

Diffuse reflectance measurements (Figure 5) on select materials showed that the band gaps were relatively unchanged except for the double doped sample **N-Nd-R/N-Nd-A**. Here the band gap was reduced from ~3.12 down towards the visible region of 2.99.

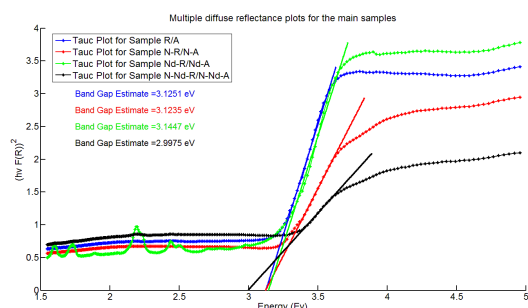


Fig. 5 Tauc plots calculated from the diffuse reflectance data showing a relatively unchanged band gap approximation between samples the only sample to show a shift in the band gap towards the visible was sample **N-Nd-R/N-Nd-A**.

Samples were evaluated for photocatalytic performance under UV (365 nm) and white light irradiation. Once the substrate was removed, nanoparticles were oven-dried and added to aqueous solutions of a dye: Rhodamine B. Rhodamine B dye is often used to mimic organic pollutants due to its similarity to aromatic organic pollutants. Rhodamine B also has a strong absorption/emission at 550 nm, which was used as the probe for the photocatalytic dye degradation studies.

It is well known that mixed-phase samples of anatase and rutile outperform the individual polymorphs in photocatalytic applications.⁴⁸ Doped samples under white light photocatalysis exhibited improved performance, with the double rutile/anatase nitrogen and neodymium doped sample giving the best performance, due to a slightly increased visible absorption window. UV photocatalytic results are summarized in Figures 5 and 6 and the raw data is given in supplementary information Figure S2 and S3.

It was found that all samples were effective at degrading the Rhodamine B (Figure 6). The single phase doped samples appears to promote photocatalytic activity whilst the dual doping seems to reduce the photocatalytic efficiency. This is evidenced by the comparison of sample **R/A** with **Nd-R/Nd-A** and the singularly doped composites. Sample **Nd-R/A** exhibited the highest activity among the Nd doped bi-phasic samples under ultraviolet light. Observation suggests that there is more at play than a simple band gap reduction when doping the anatase and the rutile. The single phase doping of the rutile (**Nd-R/A**) appears to be almost twice as effective in terms of an enhancement over the activity of the pure sample (**R/A**) as the corresponding single phase doping of the anatase (**R/Nd-A**) when doping with the neodymium.

In the nitrogen doped system it is noted that the interstitial doping of nitrogen improves photocatalytic activity, as has been seen before.^{23,29,30} Figures 6 and 7 show that the nitrogen doping is more effective in enhancing photoactivity than the neodymium at the levels given, these dye degradation experiments achieve complete decomposition and reach the base line in a shorter time. There is a clear preference for the

nitrogen doping on the anatase side of the bi-phasic composite material when examining photocatalytic enhancement. The best sample was sample **R/N-A** with an apparent doubling of the activity over the pure **R/A** when compared to **N-R/A**.

In the case of Nitrogen doping the enhancement appears to be the opposite to that observed in the Nd doping, in that the best enhancement occurs when the Anatase side of the particle is doped. The direct comparison between any sample both with and without the nitrogen doping in the anatase side shows a significant improvement in activity, i.e., sample **R/A** → **R/N-A** and sample **N-R/A** → **N-R/N-A** both show enhancement. The double-doped concept also shows enhancement in that **Nd-R/Nd-A** has lower activity than **N-Nd-R/N-Nd-A**, again indicating an increase in activity with an increase in doping. Perhaps most notable from these results of both systems is that there seems to be a tentative preference in activity enhancement whereby the rutile phase prefers the Nd doping and the anatase phase prefers the N doping site. This is likely due to the different roles that each side of the particle plays in the overall redox reaction.⁴⁸ It is understood in a mixed phase system that the different phases are performing different roles dependent on their bandgap alignments. Scanlon *et al.*⁴⁸ have shown that in the anatase rutile system the holes concentrate on the rutile whilst the electrons concentrate on the anatase. The anatase is therefore a reduction catalyst while the rutile is an oxidation catalyst. The ability to selectively dope either the reduction or the oxidation catalyst leads to selective enhancement within the system.

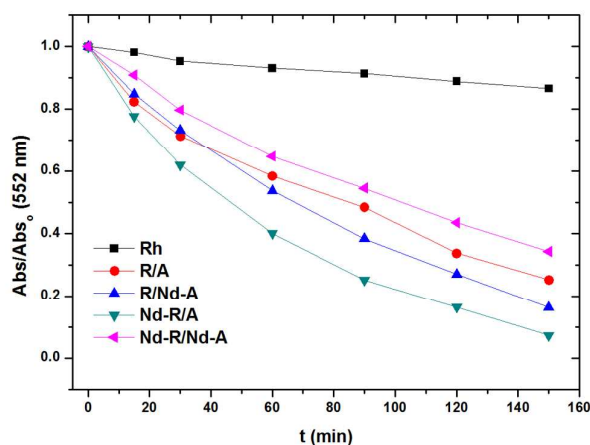


Fig. 6 Results for Rhodamine degradation; decrease in absorbance of neodymium doped samples as compared to pure titania **R/A** sample under UV light 365 nm. Reaction conditions: 25 °C, 5 mg/L Rhodamine B in water, 1 mg/L of solid and ambient air.

Under white light (Figure 7), it was shown again that both forms of doping have a significant effect on the enhancement of the TiO₂ photocatalytic activity. Once again the nitrogen has more effect and in the case of the double-doped sample, N-

Nd-R/N-Nd-A, the activity was vastly superior to any of the other samples.

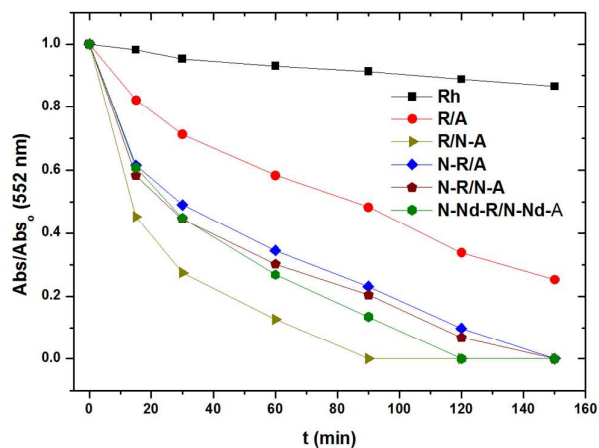


Fig. 7 Results for Rhodamine degradation; decrease in absorbance of nitrogen doped samples as compared to pure titania R/A sample under UV light 365 nm. Reaction conditions: 25 °C, 5 mg/L Rhodamine B in water, 1 mg/L of solid and ambient air.

Materials containing both nitrogen and neodymium doping agents gave the best results in the photocatalytic degradation of Rhodamine under white light. The incorporation of nitrogen into the titanium dioxide lattice has been shown to shift the band onset towards the visible region of the spectrum.^{30,80,81} The neodymium doped materials had several bands in the visible region.⁴⁰ Photocatalytic activity afforded by rutile-anatase junctions with N and Nd double doping gave the best results in organic dye degradation under white light due to a slightly increased visible absorption window and the stabilization effect of the excited state lifetime due to the synergistic relationship between the anatase and the rutile.

4. Conclusions

We have developed a new method for the synthesis of “Janus” like nanoparticles from two or more materials in contact using soluble substrates. Rutile/anatase titania composites have synergistic photocatalytic enhancement when in intimate contact.⁴³ This was demonstrated by the photocatalytic degradation of a model compound, Rhodamine B dye, under UV and white light irradiation. Dopants, such as nitrogen and neodymium, were observed to have a positive effect on white light photocatalysis and were easily incorporated into the bi-phasic nanoparticle synthesis. Such particles could have notable application in the fields of photocatalytic water cleaning or solar energy harvesting.

Acknowledgements

The Author's thank the University of Swansea and the Welsh Government Sêr Cymru Programme for funding. CWD and JCB

thank the Ramsay Trust for past and current Ramsay Fellowships. SPECIFIC and ILS at Swansea University is thanked for the use of XRD, XPS and SEM facilities.

References

- W. Shockley and H. J. Queisser, *J. Appl. Phys.*, 1961, **32**, 510–519.
- S. G. Chen, S. Chappel, Y. Diamant and A. Zaban, *Chem. Mater.*, 2001, **13**, 4629–4634.
- G. Fan, H. Zhu, K. Wang, J. Wei, X. Li, Q. Shu, N. Guo and D. Wu, *ACS Appl. Mater. Interfaces*, 2011, **3**, 721–725.
- W. Guter, J. Schöne, S. P. Philipps, M. Steiner, G. Siefer, A. Wekkeli, E. Welsler, E. Oliva, A. W. Bett and F. Dimroth, *Appl. Phys. Lett.*, 2009, **94**, 223504.
- A. Hagfeldt, G. Boschloo, L. Sun, L. Kloo and H. Pettersson, *Chem. Rev.*, 2010, **110**, 6595–6663.
- R. J. Colchester, C. A. Mosse, D. S. Bhachu, J. C. Bear, C. J. Carmalt, I. P. Parkin, B. E. Treeby, I. Papakonstantinou and A. E. Desjardins, *Appl. Phys. Lett.*, 2014, **104**, 173502.
- R. Ghosh Chaudhuri and S. Paria, *Chem. Rev.*, 2012, **112**, 2373–2433.
- T. Zhou, B. Wu and D. Xing, *J Mater Chem*, 2011, **22**, 470–477.
- K. S. Soppimath, D. C.-W. Tan and Y.-Y. Yang, *Adv. Mater.*, 2005, **17**, 318–323.
- W. Qin, D. Zhang, D. Zhao, L. Wang and K. Zheng, *Chem. Commun.*, 2010, **46**, 2304–2306.
- C. R. Crick, J. C. Bear, A. Kafizas and I. P. Parkin, *Adv. Mater.*, 2012, **24**, 3505–3508.
- G. Li and Z. Tang, *Nanoscale*, 2014, **6**, 3995–4011.
- Y. Kuwauchi, H. Yoshida, T. Akita, M. Haruta and S. Takeda, *Angew. Chem. Int. Ed.*, 2012, **51**, 7729–7733.
- J. C. Bear, N. Hollingsworth, P. D. McNaughton, A. G. Mayes, M. B. Ward, T. Nann, G. Hogarth and I. P. Parkin, *Angew. Chem. Int. Ed.*, 2014, **53**, 1598–1601.
- Z. Han, F. Qiu, R. Eisenberg, P. L. Holland and T. D. Krauss, *Science*, 2012, **338**, 1321–1324.
- S. Jun and E. Jang, *Angew. Chem. Int. Ed.*, 2013, **52**, 679–682.
- J. M. Schnorr and T. M. Swager, *Chem. Mater.*, 2011, **23**, 646–657.
- W. J. Cantwell and J. Morton, *Composites*, 1991, **22**, 347–362.
- V. Diesen, C. W. Dunnill, J. C. Bear, S. Firth, M. Jonsson and I. P. Parkin, *Chem. Vap. Depos.*, 2014, **20**, 91–97.
- Y. Natsume and H. Sakata, *Thin Solid Films*, 2000, **372**, 30–36.
- A. L. K. Tan, A. M. Soutar, I. F. Annergren and Y. N. Liu, *Surf. Coat. Technol.*, 2005, **198**, 478–482.
- G. Hyett and I. P. Parkin, *Surf. Coat. Technol.*, 2007, **201**, 8966–8970.
- C. W. Dunnill, A. Kafizas and I. P. Parkin, *Chem. Vap. Depos.*, 2012, **18**, 89–101.
- A. Fujishima and K. Honda, *Nature*, 1972, **238**, 37–38.
- R. Su, R. Tiruvalam, A. J. Logsdail, Q. He, C. A. Downing, M. T. Jensen, N. Dimitratos, L. Kesavan, P. P. Wells, R. Bechstein, H. H. Jensen, S. Wendt, C. R. A. Catlow, C. J. Kiely, G. J. Hutchings and F. Besenbacher, *ACS Nano*, 2014.

- 26 K. Maeda, N. Murakami and T. Ohno, *J. Phys. Chem. C*, 2014, **118**, 9093–9100.
- 27 P. Carmichael, D. Hazafy, D. S. Bhachu, A. Mills, J. A. Darr and I. P. Parkin, *Phys. Chem. Chem. Phys.*, 2013, **15**, 16788–16794.
- 28 S. Noimark, K. Page, J. C. Bear, C. Sotelo-Vazquez, R. Quesada-Cabrera, Y. Lu, E. Allan, J. A. Darr and I. P. Parkin, *Faraday Discuss.*, 2014.
- 29 C. W. Dunnill, K. Page, Z. A. Aiken, S. Noimark, G. Hyett, A. Kafizas, J. Pratten, M. Wilson and I. P. Parkin, *J. Photochem. Photobiol. Chem.*, 2011, **220**, 113–123.
- 30 C. W. Dunnill and I. P. Parkin, *Dalton Trans.*, 2011, **40**, 1635–1640.
- 31 C. W. Dunnill, Z. Ansari, A. Kafizas, S. Perni, D. J. Morgan, M. Wilson and I. P. Parkin, *J. Mater. Chem.*, 2011, **21**, 11854–11861.
- 32 A. Kafizas, C. W. Dunnill and I. P. Parkin, *J. Mater. Chem.*, 2010, **20**, 8336–8349.
- 33 A. Kafizas, C. W. Dunnill and I. P. Parkin, *Phys. Chem. Chem. Phys.*, 2011, **13**, 13827–13838.
- 34 U. Bach, D. Lupo, P. Comte, J. E. Moser, F. Weissörtel, J. Salbeck, H. Spreitzer and M. Grätzel, *Nature*, 1998, **395**, 583–585.
- 35 P. K. Nayak and D. Cahen, *Adv. Mater.*, 2014, **26**, 1622–1628.
- 36 S. K. Pathak, A. Abate, P. Ruckdeschel, B. Roose, K. C. Gödel, Y. Vaynzof, A. Santhala, S.-I. Watanabe, D. J. Hollman, N. Noel, A. Sepe, U. Wiesner, R. Friend, H. J. Snaith and U. Steiner, *Adv. Funct. Mater.*, 2014, **24**, 6046–6055.
- 37 R. W. Matthews, *Sol. Energy*, 1987, **38**, 405–413.
- 38 C. Gao, Z. Sun, K. Li, Y. Chen, Y. Cao, S. Zhang and L. Feng, *Energy Environ. Sci.*, 2013, **6**, 1147–1151.
- 39 V. Likodimos, C. Han, M. Pelaez, A. G. Kontos, G. Liu, D. Zhu, S. Liao, A. A. de la Cruz, K. O'Shea, P. S. M. Dunlop, J. A. Byrne, D. D. Dionysiou and P. Falaras, *Ind. Eng. Chem. Res.*, 2013, **52**, 13957–13964.
- 40 V. Gomez, A. M. Balu, J. C. Serrano-Ruiz, S. Irusta, D. D. Dionysiou, R. Luque and J. Santamaría, *Appl. Catal. Gen.*, 2012, **441–442**, 47–53.
- 41 X. Z. Li and F. B. Li, *Environ. Sci. Technol.*, 2001, **35**, 2381–2387.
- 42 M. A. Tarselli, *Nat. Chem.*, 2013, **5**, 546–546.
- 43 M. Ni, M. K. H. Leung, D. Y. C. Leung and K. Sumathy, *Renew. Sustain. Energy Rev.*, 2007, **11**, 401–425.
- 44 A. L. Linsebigler, G. Lu and J. T. Yates, *Chem. Rev.*, 1995, **95**, 735–758.
- 45 T. Kawahara, Y. Konishi, H. Tada, N. Tohge, J. Nishii and S. Ito, *Angew. Chem.*, 2002, **114**, 2935–2937.
- 46 Y. K. Kho, A. Iwase, W. Y. Teoh, L. Mädler, A. Kudo and R. Amal, *J. Phys. Chem. C*, 2010, **114**, 2821–2829.
- 47 J. Zhang, Q. Xu, Z. Feng, M. Li and C. Li, *Angew. Chem. Int. Ed.*, 2008, **47**, 1766–1769.
- 48 D. O. Scanlon, C. W. Dunnill, J. Buckeridge, S. A. Shevlin, A. J. Logsdail, S. M. Woodley, C. R. A. Catlow, M. J. Powell, R. G. Palgrave, I. P. Parkin, G. W. Watson, T. W. Keal, P. Sherwood, A. Walsh and A. A. Sokol, *Nat. Mater.*, 2013, **12**, 798–801.
- 49 R. Quesada-Cabrera, C. Sotelo-Vazquez, J. C. Bear, J. A. Darr and I. P. Parkin, *Adv. Mater. Interfaces*, 2014, **1**, n/a–n/a.
- 50 C. W. Dunnill and I. P. Parkin, *Chem. Vap. Depos.*, 2009, **15**, 171–174.
- 51 C. W. Dunnill, Z. A. Aiken, A. Kafizas, J. Pratten, M. Wilson, D. J. Morgan and I. P. Parkin, *J. Mater. Chem.*, 2009, **19**, 8747–8754.
- 52 X. Chen and S. S. Mao, *Chem Rev*, 2007, **107**, 2891–2959.
- 53 L. G. Devi and B. N. Murthy, *Catal. Lett.*, 2008, **125**, 320–330.
- 54 Y. Shen, T. Xiong, H. Du, H. Jin, J. Shang and K. Yang, *J. Sol-Gel Sci. Technol.*, 2009, **50**, 98–102.
- 55 N. Couselo, F. S. García Einschlag, R. J. Candal and M. Jobbágy, *J. Phys. Chem. C*, 2008, **112**, 1094–1100.
- 56 S. Klosek and D. Raftery, *J. Phys. Chem. B*, 2001, **105**, 2815–2819.
- 57 J. Lukáč, M. Klementová, P. Bezdička, S. Bakardjieva, J. Šubr, L. Szatmáry, Z. Bastl and J. Jirkovský, *Appl. Catal. B Environ.*, 2007, **74**, 83–91.
- 58 K. T. Ranjit and B. Viswanathan, *J. Photochem. Photobiol. Chem.*, 1997, **108**, 79–84.
- 59 X. Yang, C. Cao, L. Erickson, K. Hohn, R. Maghirang and K. Klabunde, *Appl. Catal. B Environ.*, 2009, **91**, 657–662.
- 60 G. Colón, M. Maicu, M. C. Hidalgo and J. A. Navío, *Appl. Catal. B Environ.*, 2006, **67**, 41–51.
- 61 H. Wei, Y. Wu, N. Lun and F. Zhao, *J. Mater. Sci.*, 2004, **39**, 1305–1308.
- 62 V. Gomez, A. Clemente, S. Irusta, F. Balas and J. Santamaría, *Environ. Sci. Nano*, 2014, **1**, 496–503.
- 63 Q. Yao, J. Liu, Q. Peng, X. Wang and Y. Li, *Chem. – Asian J.*, 2006, **1**, 737–741.
- 64 S. Bingham and W. A. Daoud, *J. Mater. Chem.*, 2011, **21**, 2041–2050.
- 65 S. I. Shah, W. Li, C.-P. Huang, O. Jung and C. Ni, *Proc. Natl. Acad. Sci. U. S. A.*, 2002, **99 Suppl 2**, 6482–6486.
- 66 J. Li, X. Yang, X. Yu, L. Xu, W. Kang, W. Yan, H. Gao, Z. Liu and Y. Guo, *Appl. Surf. Sci.*, 2009, **255**, 3731–3738.
- 67 B. Shahmoradi, I. A. Ibrahim, N. Sakamoto, S. Ananda, R. Somashekar, T. N. G. Row and K. Byrappa, *J. Environ. Sci. Health Part A*, 2010, **45**, 1248–1255.
- 68 Joseph C. Beara, Virginia Gomeza, Nikolaos S. Kefallinos James D. McGettrick, Andrew R. Barron, Charles W. Dunnill, *Journal of Colloid and Interface Science*. 460, 2015 Pages 29–35.
- 69 M. J. Powell, C. W. Dunnill and I. P. Parkin, *J. Photochem. Photobiol. Chem.*, 2014, **281**, 27–34.
- 70 C. W. Dunnill, *International Journal of Photoenergy* 2014, 2014, 5.
- 71 S. Rengaraj, S. Venkataraj, J.-W. Yeon, Y. Kim, X. Z. Li and G. K. H. Pang, *Appl. Catal. B Environ.*, 2007, **77**, 157–165.
- 72 NIST X-Ray Photoelectron Spectrosc. XPS Database Version 35.
- 73 N. R. Khalid, E. Ahmed, Z. Hong, Y. Zhang, M. Ullah and M. Ahmed, *Ceram. Int.*, 2013, **39**, 3569–3575.
- 74 M. Sathish, B. Viswanathan, R. P. Viswanath and C. S. Gopinath, *Chem. Mater.*, 2005, **17**, 6349–6353.
- 75 J. F. Moulder, W. F. Stickle, P. E. Sobol and K. D. Bomben, *Handbook of X Ray Photoelectron Spectroscopy: A Reference Book of Standard Spectra for Identification and Interpretation of Xps Data*, Physical Electronics, Eden Prairie, Minn, 1995.
- 76 M. Yuan, J. Zhang, S. Yan, G. Luo, Q. Xu, X. Wang and C. Li, *J. Alloys Compd.*, 2011, **509**, 6227–6235.
- 77 D. F. Mullica, C. K. C. Lok, H. O. Perkins, G. A. Benesh and V. Young, *J. Electron Spectrosc. Relat. Phenom.*, 1995, **71**, 1–20.

Journal Name

ARTICLE

78. K. Kataoka, J. Awaka, N. Kijima, H. Hayakawa, K. Ohshima and J. Akimoto, *Chem. Mater.*, 2011, **23**, 2344–2352.
79. K. Kiatkittipong, A. Iwase, J. Scott and R. Amal, *Chem. Eng. Sci.*, 2013, **93**, 341–349.
80. C. W. Dunnill, Z. Aiken, J. Pratten, M. W. Wilson and I. Parkin, *ECS Trans.*, 2009, **25**, 65–72.
81. C. W. Dunnill, Z. A. Aiken, J. Pratten, M. Wilson and I. P. Parkin, *Chem. Vap. Depos.*, 2010, **16**, 50–54.